
HOKKAIDO UNIVERSITY

Title	Highly conducting leakage-free electrolyte for SrCoOx-based non-volatile memory device
Author(s)	Katase, Takayoshi; Suzuki, Yuki; Ohta, Hiromichi
Citation	Journal of Applied Physics, 122(13), 135303 https://doi.org/10.1063/1.5005520
Issue Date	2017-10-07
Doc URL	http://hdl.handle.net/2115/71636
Rights	The following article appeared in Takayoshi Katase, Yuki Suzuki and Hiromichi Ohta, Highly conducting leakage-free electrolyte for SrCoOx-based non-volatile memory device, Journal of Applied Physics 122, 135303 (2017), doi: 10.1063/1.5005520 and may be found at http://aip.scitation.org/doi/abs/10.1063/1.5005520 .
Type	article
File Information	1.5005520.pdf


Instructions for use

Hokkaido University Collection of Scholarly and Academic Papers : HUSCAP

Highly conducting leakage-free electrolyte for $SrCoO_X$-based non-volatile memory device

Takayoshi Katase, Yuki Suzuki, and Hiromichi Ohta

Citation: Journal of Applied Physics **122**, 135303 (2017);
View online: https://doi.org/10.1063/1.5005520
View Table of Contents: http://aip.scitation.org/toc/jap/122/13
Published by the American Institute of Physics

Articles you may be interested in

Solid-phase epitaxial film growth and optical properties of a ferroelectric oxide, $Sr_2Nb_2O_7$
Journal of Applied Physics **122**, 135305 (2017); 10.1063/1.4997813

Hall measurements on low-mobility thin films
Journal of Applied Physics **122**, 135306 (2017); 10.1063/1.4990470

The anisotropic size effect of the electrical resistivity of metal thin films: Tungsten
Journal of Applied Physics **122**, 135301 (2017); 10.1063/1.5004118

Thermoelectric phase diagram of the $SrTiO_3$–$SrNbO_3$ solid solution system
Journal of Applied Physics **121**, 185102 (2017); 10.1063/1.4983359

Theory of energy and power flow of plasmonic waves on single-walled carbon nanotubes
Journal of Applied Physics **122**, 133103 (2017); 10.1063/1.4997454

Anisotropic large magnetoresistance in $TaTe_4$ single crystals
Journal of Applied Physics **122**, 135101 (2017); 10.1063/1.5005907

Highly conducting leakage-free electrolyte for $SrCoO_x$-based non-volatile memory device

Takayoshi Katase,[1,2,3,a)] Yuki Suzuki,[4] and Hiromichi Ohta[1,a)]
[1]*Research Institute for Electronic Science, Hokkaido University, N20W10, Kita, Sapporo 001-0020, Japan*
[2]*Laboratory for Materials and Structures, Institute of Innovative Research, Tokyo Institute of Technology, 4259 Nagatsuta, Midori, Yokohama 226-8503, Japan*
[3]*PRESTO, Japan Science and Technology Agency, 7, Gobancho, Chiyoda, Tokyo 102-0076, Japan*
[4]*School of Information Science and Technology, Hokkaido University, N14W19, Kita, Sapporo 060-0814, Japan*

(Received 28 May 2017; accepted 17 September 2017; published online 3 October 2017)

The electrochemical switching of $SrCoO_x$-based non-volatile memory with a thin-film-transistor structure was examined by using liquid-leakage-free electrolytes with different conductivities (σ) as the gate insulator. We first examined leakage-free water, which is incorporated in the amorphous (a-) $12CaO{\cdot}7Al_2O_3$ film with a nanoporous structure (Calcium Aluminate with Nanopore), but the electrochemical oxidation/reduction of the $SrCoO_x$ layer required the application of a high gate voltage (V_g) up to 20 V for a very long current-flowing-time (t) ~40 min, primarily due to the low σ [2.0×10^{-8} S cm^{-1} at room temperature (RT)] of leakage-free water. We then controlled the σ of the leakage-free electrolyte, infiltrated in the a-Na_xTaO_3 film with a nanopillar array structure, from 8.0×10^{-8} S cm^{-1} to 2.5×10^{-6} S cm^{-1} at RT by changing the $x = 0.01$–1.0. As the result, the t, required for the metallization of the $SrCoO_x$ layer under small $V_g = -3$ V, becomes two orders of magnitude shorter with increase of the σ of the a-Na_xTaO_3 leakage-free electrolyte. These results indicate that the ion migration in the leakage-free electrolyte is the rate-determining step for the electrochemical switching, compared to the other electrochemical process, and the high σ of the leakage-free electrolyte is the key factor for the development of the non-volatile $SrCoO_x$-based electro-magnetic phase switching device. *Published by AIP Publishing.* https://doi.org/10.1063/1.5005520

I. INTRODUCTION

Transition metal oxides (TMOs) have been expected as an active material for novel functional devices, because they exhibit a rich variety of physical properties, such as metal-insulator transition, magnetic transition, electrochromism, and superconductivity.[1–5] The variation of the functional properties in TMOs originates from the flexibility of the valence state of TM ions.[6] By changing the number of d electrons in TM ions, the TMOs show dramatic changes in the optical, electronic, and magnetic properties through phase transitions.[7]

Strontium cobaltite ($SrCoO_x$) shows distinct electro-magnetic properties depending on the valence state of the Co ion.[8,9] The oxygen off-stoichiometry (x) in $SrCoO_x$ can be varied in the range of 2.5–3.0, where the oxygen-vacant $SrCoO_{2.5}$ phase has a brownmillerite (BM-) type structure and the fully-oxidized $SrCoO_3$ phase has a simple perovskite (P-) type structure. The BM-$SrCoO_{2.5}$ with Co^{3+} ($3d^6$) is an antiferromagnetic (AFM) insulator with a Néel temperature of 570 K,[8] whereas the P-$SrCoO_3$ with Co^{4+} ($3d^5$) is a ferromagnetic (FM) metal with a Curie temperature of 275 K.[10] The highly contrastive ground states between the AFM insulator and FM metal should be promising for novel electro-magnetic phase switching devices.

In order to modulate their electron-magnetic properties, there are two approaches for the control of x in $SrCoO_x$. High-temperature heat treatment under oxidative/reductive conditions has been a conventional way to control the x of TMOs.[11–13] For $SrCoO_x$ thin films, the two phases could be altered reversibly at least 200–300 °C,[14,15] but the heating process for the phase switching is unsuited for the device operating at room temperature (RT). Meanwhile, the redox reaction using a liquid electrolyte is another classical method for the control of x at RT;[16] the reversible redox reaction of $SrCoO_x$ has been accomplished by the electrolysis in alkaline aqueous solutions.[17–21] However, it cannot be used for practical purposes without sealing; the electro-magnetic phase switching should be operatable in a solid-state device at RT.

In order to overcome this issue, we have proposed liquid-leakage-free electrolytes incorporated in nanoporous insulators. In 2010, we have developed an amorphous (a-) $12CaO{\cdot}7Al_2O_3$ film with a nanoporous structure (Calcium Aluminate with Nanopore, CAN) as a leakage-free water.[22] The CAN is a glassy solid film containing nanopores with average diameters of 10–20 nm. Water vapor in air is automatically absorbed into the nanopores due to capillary action and the percolation conduction of water can be observed in the interconnected nanopores. We further developed an a-$NaTaO_3$ film with a nanopillar array structure, which works as a leakage-free electrolyte containing an alkali hydroxide as a salt.[23] Also for this case, the water vapor in air is absorbed into the interspace of nanopillar arrays and then, a small amount of Na^+ ions from the a-$NaTaO_3$ nanopillars is dissolved into the adsorbed water, leading to the NaOH aqueous solution infiltrated in the solid a-$NaTaO_3$ film. Thus, no leakage of the electrolyte occurs due to the large surface tension

a)Authors to whom correspondence should be addressed: katase@mces.titech.ac.jp and hiromichi.ohta@es.hokudai.ac.jp

of the electrolyte/nanopores; i.e., the formation of a liquid-leakage-free electrolyte.

Recently, we demonstrated an electrochemically switchable electro-magnetic phase switching device of $SrCoO_x$ by using a three terminal thin-film transistor (TFT) structure with the leakage-free electrolyte.[23–26] The TFT structure is composed of a $SrCoO_x$ film as an active channel layer and a a-$NaTaO_3$ film with a nanopillar array structure as a gate insulator. By applying the gate voltage, the electrochemical oxidation/reduction occurs and the reversible switching between the AFM insulator and FM metal of the $SrCoO_x$ layer was realized under a small DC voltage (± 3 V) within a very short time (2–3 s) at RT in air.[24] The electrochemical reaction of the $SrCoO_x$ layer obeys the Faraday's laws of electrolysis and the device operation can be controlled by the current density flowing in the device. Therefore, it is considered that the conductivity of the leakage-free electrolyte is the key factor for the electrochemical switching of $SrCoO_x$-based TFT, but the conductivity control of the leakage-free electrolyte and their effects on the device operation has not been examined yet; the systematic characterization should lead to the further understanding for the electrochemical switching of $SrCoO_x$-based TFT.

In this paper, we examined the electrochemical switching of $SrCoO_x$ TFT by using liquid-leakage-free electrolytes of the CAN film and a-Na_xTaO_3 films with different conductivities. We fabricated the a-Na_xTaO_3 films with different $x = 0.01$–1.0, to demonstrate the conductivity control of the leakage-free electrolyte. As the result, the conductivity of a-Na_xTaO_3 films can be largely controlled from 8.0×10^{-8} S cm^{-1} ($x = 0.01$) to 2.5×10^{-6} S cm^{-1} ($x = 1$) at RT, compared to the 2.0×10^{-8} S cm^{-1} of the CAN film. We examined the effect of the different conductivity of the leakage-free electrolytes on the device operation.

II. EXPERIMENTAL

A. Fabrication of leakage-free electrolytes

The leakage-free electrolytes of the CAN film and Na_xTaO_3 films were fabricated by pulsed laser deposition (PLD) at RT. A KrF excimer laser (wavelength of 248 nm, repetition rate of 10 Hz) was used to ablate the targets of $12CaO{\cdot}7Al_2O_3$ and Na_xTaO_3 ceramics. In order to control the Na concentration (x) in the Na_xTaO_3 films, the chemical composition of the targets of Na_xTaO_3, which is mixture of $NaTaO_3$ and Ta_2O_5 phases, was changed in the range of $x = 0.01$–1.0.

B. Fabrication of $SrCoO_x$-TFT with a leakage-free electrolyte

Figure 1 schematically illustrates the TFT structure with a 800-μm-long and 400-μm-wide channel, which is fabricated using stencil masks onto an atomically-flat stepped-and-terraced surface of a $SrCoO_{2.5}$ epitaxial film;[24] the 30-nm-thick $SrCoO_{2.5}$ layer was deposited on a (001) $SrTiO_3$ single crystal (substrate size: $10 \times 10 \times 0.5$ mm^3) at 720 °C under an oxygen pressure (P_{O2}) of 10 Pa by PLD. A 20-nm-thick Cr/Au bilayer film, which served as the source and drain electrode for the ohmic contant to the $SrCoO_x$ layer,

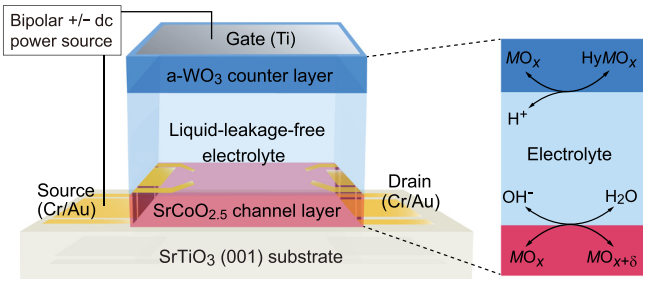

FIG. 1. A schematic of three-terminal TFT structure consisting of a $SrCoO_{2.5}$ channel layer, a liquid-leakage-free electrolyte as a gate insulator, an a-WO_3 counter layer, and a Ti gate electrode on a $SrTiO_3$ (001) substrate. Cr/Au bilayer films were used for source-drain electrodes. The right figure illustrates the electrochemical reaction in the device during the gate voltage application.

was deposited by electron beam (EB) evaporation at RT. The liquid-leakage-free electrolytes of the 160-nm-thick CAN film and 300-nm-thick Na_xTaO_3 films were deposited on the $SrCoO_{2.5}$ layer. Finally, a 20-nm-thick a-WO_3 counter layer and a Ti gate electrode were, respectively, deposited by PLD and EB evaporation on the leakage-free electrolyte. By applying the negative gate voltage (V_g), the OH^- ion is attracted to the surface of the $SrCoO_x$ layer and electrochemical oxidation occurs. Meanwhile, by applying the positive V_g, the reverse reaction occurs for the reduction of the $SrCoO_x$ layer. The a-WO_3 counter layer works as the H^+ absorber,[27] which maintains a better electrochemical balance in the device.

C. Characterization

The film density of the leakage-free electrolytes was characterized by X-ray reflectivity measurement, and the film porosity (Φ) was calculated from the ratio of the densities of porous and dense films. The cross-sectional microstructure of thin films was examined by high-resolution transmission electron microscopy (TEM) and scanning TEM (JEM-ARM200F, 200 kV, JEOL Ltd.). The cross-sectional samples for TEM observations were prepared by the focused-ion-beam (FIB) micro-sampling technique, in which the multilayer structure region of the TFTs was cutout and thinned by FIB (FB-2000A, HITACHI).

The conductivity (σ) of the leakage-free electrolytes was measured by the AC impedance method using an impedance analyzer (YHP4192A, Yokogawa-Hewlett-Packard) and a potentio/galvanostat (VersaSTAT 4, Princeton Applied Research ltd.), where the films were sandwiched by Au electrodes and the σ was measured perpendicular to the thin-film plane. The σ was estimated from the intercept on the real axis of the semicircle in the Cole–Cole plots.

The $SrCoO_x$-TFT characteristics were examined by measuring the sheet resistance (R_s) and thermopower (S), after applying V_g and subsequently switching the V_g off, at RT in air. The V_g is applied between the gate-source electrodes of the device. The gate current (I_g) during the V_g application was measured by a source measurement unit (Keithley 2450). The R_s was measured by d.c. four probe method in the van der Pauw electrode configuration. The S was measured by giving a temperature difference (ΔT) of 5 K in the film using two Peltier devices, where the actual temperatures

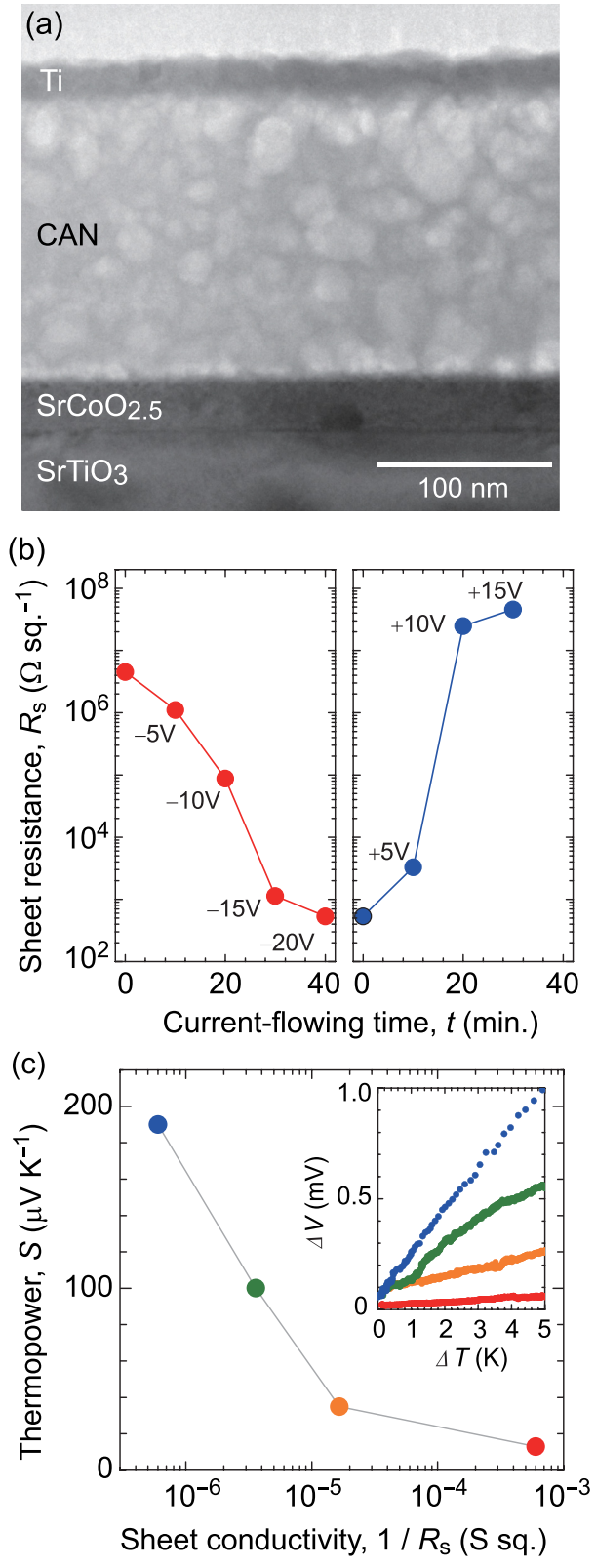

FIG. 2. (a) Cross-sectional TEM image of the $SrCoO_x$ TFT with leakage-free water. The trilayer structure composed of $SrCoO_{2.5}$ (30 nm), CAN (160 nm), and Ti (20 nm) layers is clearly seen. Many light spots in the CAN layer indicate nanopores, which are fully occupied with water. (b) R_s *vs.* current-flowing time (t) of applied V_g for the $SrCoO_x$ layer. The R_s was measured after the V_g application, where negative V_g up to –20 V was applied for oxidation (left panel) and positive V_g up to +15 V was applied for reduction (right panel) of the $SrCoO_x$ layer. The V_g application time was 10 min at each step. (c) S *vs.* $1/R_s$ at RT. ΔV–ΔT plots are shown in the inset.

of both sides of the $SrCoO_x$ layer were monitored by two tiny thermocouples. The thermo-electromotive force (ΔV) and ΔT were simultaneously measured, and the S was obtained from the slope of the ΔV–ΔT plot.

III. RESULTS AND DISCUSSIONS

A. $SrCoO_x$ TFT with leakage-free water

We first fabricated the $SrCoO_x$ TFT with leakage-free water. The CAN film was deposited at RT under a P_{O2} of

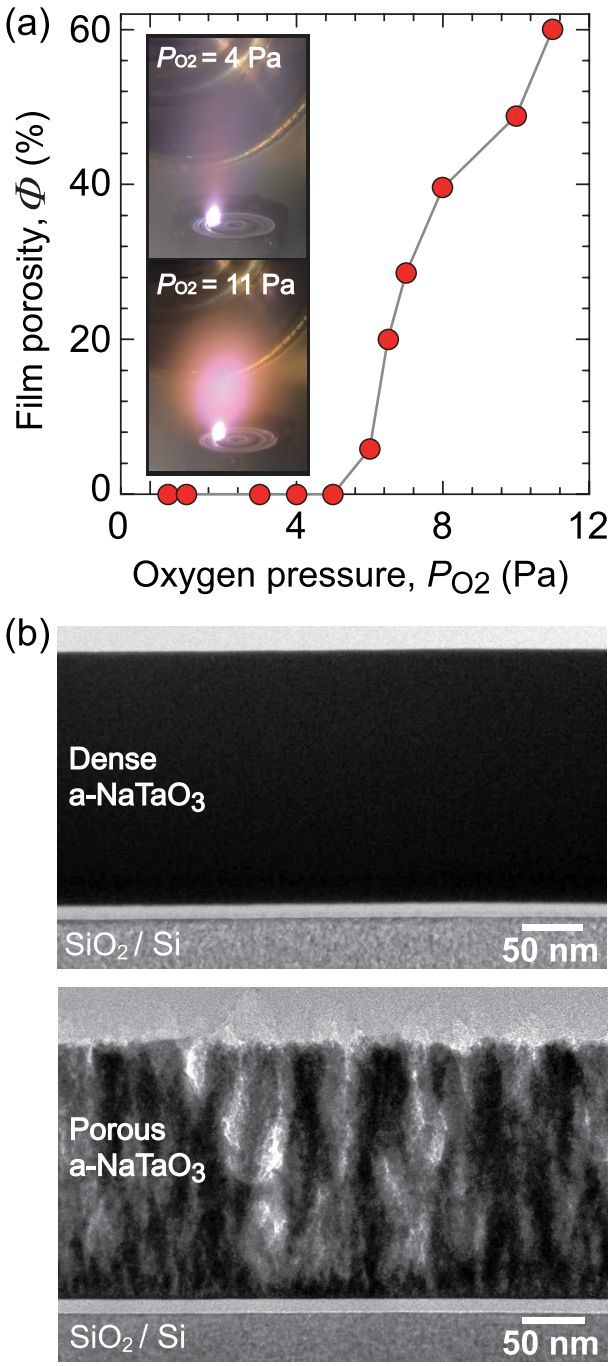

FIG. 3. Microstructure analyses of a-$NaTaO_3$ film. (a) Film porosity (Φ) as a function of oxygen pressure (P_{O2}) during the deposition at RT. The insets show the pictures of ablation plume of $NaTaO_3$ under $P_{O2} = 4$ Pa and 11 Pa. (b) BF-STEM images of a dense a-$NaTaO_3$ film (upper panel) and a porous a-$NaTaO_3$ film (lower panel), deposited on SiO_2/Si substrates at $P_{O2} = 4$ Pa and 11 Pa, respectively.

5 Pa by PLD, because the film density of the CAN film can be controlled by the P_{O2} during the deposition and the film porosity (Φ) at $P_{O2} = 5$ Pa was 32%.[28] The σ of the 200-nm-thick CAN film was measured to be 2.0×10^{-8} S cm^{-1} at RT. Considering that the water is fully occupied in the nanopore region (32% of the total volume of CAN film), the σ of water in the CAN film is estimated to be 6.3×10^{-8} S cm^{-1}, which is consistent with 5.6×10^{-8} S cm^{-1} of the ultrapure water.[29] Figure 2(a) shows the high-resolution TEM image of the cross-sectional $SrCoO_x$ TFT, where the electron incident direction was $SrTiO_3$ [110]. The multilayered structure composed of $SrCoO_{2.5}$ (30 nm)/CAN (160 nm)/Ti (20 nm) was observed and the numerous light spots with diameters of 10–20 nm are seen in the CAN film, indicating the presence of high-density nanopores.

The electrochemical switching of the $SrCoO_x$ TFT with leakage-free water was examined by measuring R_s and S at RT. Figure 2(b) shows the variation of R_s with respect to the current-flowing time (t) under various V_g, where the R_s was measured immediately after the bias application for 10 min at each V_g. First, a negative V_g up to –20 V was applied for the oxidation of the $SrCoO_{2.5}$ layer (left panel), and then a positive V_g up to +15 V was applied for the reduction (right panel). The R_s decreased from 4.5 MΩ sq.$^{-1}$ at the initial state down to 0.5 kΩ sq.$^{-1}$ at $V_g = -20$ V, due to the oxidation of the $SrCoO_{2.5}$ film. Subsequently, by applying a positive V_g up to +15 V, the R_s recovered to the insulating state (46 MΩ sq.$^{-1}$) due to the reduction. Figure 2(c) summarizes the S with respect to the sheet conductivity ($1/R_s$). The ΔV–ΔT plots at RT are shown in the inset of Fig. 2(c), which ensures a linear relationship between ΔV and ΔT. The measured S are always positive, indicating that the $SrCoO_x$ layer is a p-type conductor. The S decreased form +190 μV K^{-1} to +10 μV K^{-1}, which is almost the same with that of the metallic $SrCoO_3$ phase.[14] Since the S basically reflects the energy differential of the density of states (DOS) around the Fermi level (E_F), $[\frac{\partial DOS(E)}{\partial E}]_{E=EF}$,[30,31] the decrease of S with increase of $1/R_s$ reflect the electronic-structure change from the insulating to metallic state of the $SrCoO_x$ layer by oxidation. However, these results imply that the electrochemical switching of $SrCoO_x$ TFT with leakage-free water requires the application of high V_g up to 20 V for a very long $t \sim 40$ min, which should be necessary to gain the enough coulomb density for the electrochemical reaction of the $SrCoO_x$ layer, primarily due to the low σ of the leakage-free water.[32]

B. Conductivity control of leakage-free electrolyte

We then examined the conductivity control of leakage-free electrolyte by changing x of a-Na_xTaO_3 films. The a-Na_xTaO_3 films with nominal $x = 0.01$, 0.1, and 1.0 were deposited at RT by PLD. Figure 3(a) summarizes the Φ of a-$NaTaO_3$ films with respect to P_{O2} during the deposition. When the P_{O2} exceeds 4 Pa, the plume becomes large, as shown in the inset. With the increase of $P_{O2} > 5$ Pa, the film density steeply starts to decrease, leading to the formation of a porous a-$NaTaO_3$ film (Supplementary material, Figs. S1 and S2) and the Φ reached to 60% at $P_{O2} = 11$ Pa. Figure 3(b) shows the bright field (BF) STEM image of the a-$NaTaO_3$ films fabricated at a P_{O2} of 4 and 11 Pa. Although the a-$NaTaO_3$ film fabricated at a low P_{O2} of 4 Pa is fully dense, that grown under a high P_{O2} of 11 Pa has a nanopillar array structure. Figures 4(a)–4(c) summarize the impedance plots at RT in air for the 300-nm-thick a-Na_xTaO_3 films ($x = 0.01$–1.0) with a nanopillar array structure, fabricated at $P_{O2} = 11$ Pa. The semicircle was observed at the high frequency region ≥ 10 kHz but slightly distorted presumably because the a-Na_xTaO_3 is not a pure capacitor. In order to estimate the σ, we fitted the semicircle by using the equivalent circuit model composed of a constant phase element and ionic resistance in parallel. The estimated σ of a-Na_xTaO_3 films was largely controlled from 5.2×10^{-8} S cm^{-1} ($x = 0.01$) to 1.2×10^{-7} S cm^{-1} ($x = 0.1$) to 2.8×10^{-6} S cm^{-1} ($x = 1$), compared to 2.0×10^{-8} S cm^{-1} of the CAN film, indicating that the change of x in a-Na_xTaO_3 film realized the control of σ of the leakage-free electrolyte.

C. $SrCoO_x$-TFT using leakage-free electrolyte with different conductivity

In order to compare the electrochemical switching properties of $SrCoO_x$ TFT using the gate insulator of a-Na_xTaO_3 films with different conductivities, we investigated the

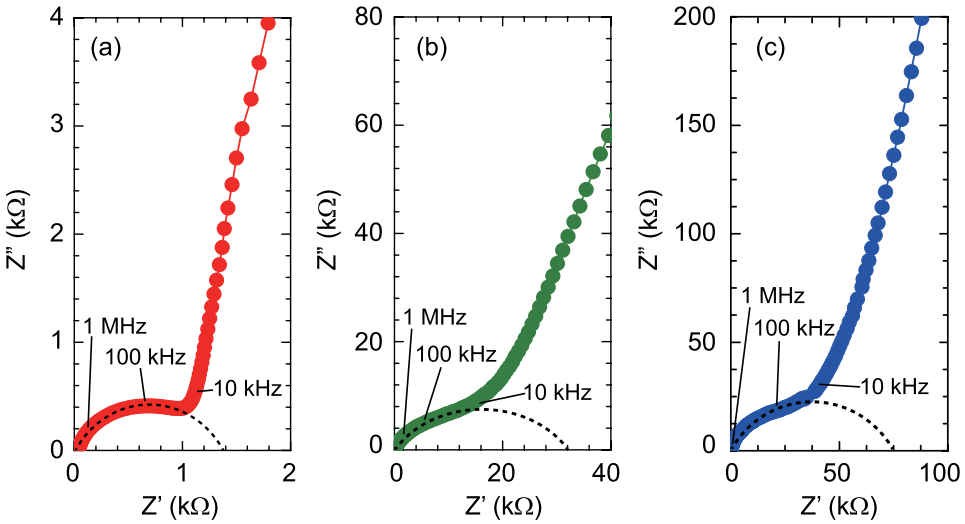

FIG. 4. Cole–Cole plots of 300-nm-thick a-Na_xTaO_3 films (950 μm × 800 μm) with $x = 1.0$ (a), 0.1 (b), and 0.01 (c), measured at RT in air. The dotted lines are fitting curves by using the equivalent circuit model composed of the constant phase element and ionic resistance in parallel.

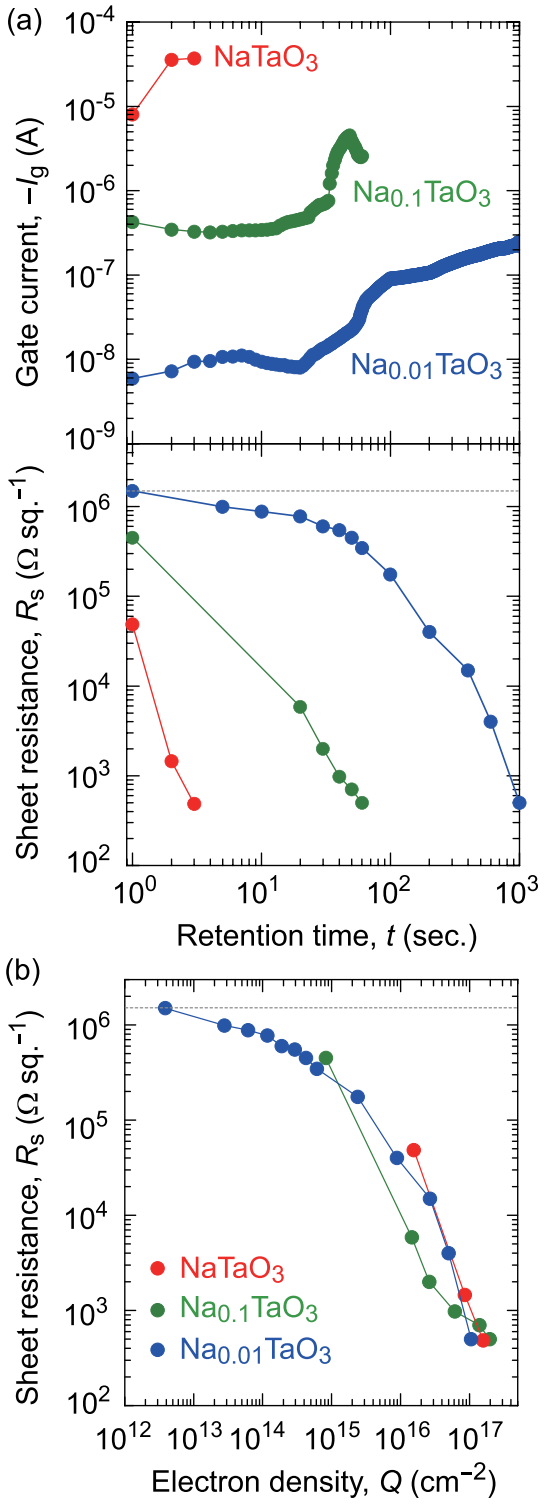

FIG. 5. (a) Current-flowing time (t) dependence of I_g (upper panel) and R_s (lower panel) for the $SrCoO_x$ TFT with a-Na_xTaO_3 ($x = 0.01$, 0.1, and 1.0) leakage-free electrolyte under the application of $V_g = -3$ V. The I_g and R_s were, respectively, measured during and after the V_g application. The dotted lines indicate the R_s of the virgin $SrCoO_{2.5}$ layer. (b) Electron-density (Q) dependence of R_s under the V_g application. The Q was calculated as the integrated value of the I_g–t plots in (a).

relationship between the flowing I_g and R_s under the V_g applications. Figure 5(a) shows the variation of I_g and R_s with respect to the t of $V_g = -3$ V. For all the $SrCoO_x$ TFTs with 300-nm-thick a-Na_xTaO_3 ($x = 0.01$–1.0) gate insulators, $-I_g$ increased with t and the R_s simultaneously decreased by applying the V_g, indicating the electrochemical oxidation of the $SrCoO_x$ layer. Meanwhile, the t required for the metallization of the 30-nm-thick $SrCoO_x$ layer becomes two orders of magnitude shorter with increase of the σ of a-Na_xTaO_3 gate insulator. The time scale of the electrochemical switching can be considered to depend on ion migration in the electrolyte, electric double layer formation, electrochemical surface reaction, and O^{2-} ion diffusion into the $SrCoO_x$ layer under the V_g application. Considering that the σ of a-Na_xTaO_3 leakage-free electrolyte largely determines the time scale of the electrochemical switching, the switching strongly depends on the density of OH^- ions accumulated at the $SrCoO_x$ surface. These results suggest that the ion migration in the leakage-free electrolyte is the rate-determining step for the device operation, compared to the other electrochemical process. Therefore, the high σ of the leakage-free electrolyte is the key factor for the electrochemical switching of $SrCoO_x$ TFT.

It should be noted that the R_s does not start to decrease until the I_g increase up to a certain value. Since the V_g is applied between the gate-source electrodes, the $SrCoO_x$ layer first becomes metallic around the source electrode, and then, the metallic region gradually expands toward the drain electrode. Therefore the I_g increases with increase of t. Finally, the metallic parallel-plate structure is formed, and the I_g effectively flows at the entire region, which decreases the R_s of $SrCoO_x$ layer.

Figure 5(b) compares the variation of R_s with electron density (Q), as calculated from the integral value of the I_g–t plots in Fig. 5(a). The R_s decreased along the universal line and the oxidation processes were completed at $\sim 1.0 \times 10^{17}\,cm^{-2}$, which corresponds with the ideal Q of $1.1 \times 10^{17}\,cm^{-2}$ required for the electrochemical oxidation form $SrCoO_{2.5}$ to $SrCoO_3$ ($SrCoO_{2.5} + 2xOH^- \leftrightarrows SrCoO_{2.5+x} + xH_2O + 2xe^-$ ($0 \le x \le 0.5$)). The universal change in R_s, regardless of the σ of a-Na_xTaO_3 gate insulator, indicates that all the provided electrons were used for the electrochemical redox reaction of the $SrCoO_x$ layer, obeying Faraday's laws of electrolysis, and that the device operation can be controlled by current density.

It should be commented here that the present results are still not enough to show the feasibility for their application to the non-volatile memory device utilizing insulator/metal ferromagnet transition of $SrCoO_x$, where the device retention and endurance should be demonstrated and improved by the optimization of device structure and/or surface protection for repetitive electrochemical-switching of the $SrCoO_x$ layer. Such tests will be performed in the future studies.

IV. CONCLUSIONS

In summary, the electrochemical switching of $SrCoO_x$ TFTs was examined by using the leakage-free electrolytes with different σ as the gate insulator. We first examined the $SrCoO_x$ TFT with a water-infiltrated CAN gate insulator, but the switching required the application of high V_g up to 20 V for a very long $t = \sim 40$ min, primarily due to the low σ of the leakage-free water. We then fabricated the a-Na_xTaO_3

film with different $x = 0.01$–1.0 and demonstrated the control of σ from 8.0×10^{-8} S cm^{-1} ($x = 0.01$) to 2.5×10^{-6} S cm^{-1} ($x = 1$) at RT, compared to the 2.0×10^{-8} S cm^{-1} of the CAN film. As the result, the t at small $V_g = -3$ V, required for the metallization of the $SrCoO_x$ layer, becomes two orders of magnitude shorter with increase of the σ of the a-Na_xTaO_3 leakage-free electrolytes. These results indicate that the ion migration in the leakage-free electrolyte is the rate-determining step for the device operation, compared to the other electrochemical process, and the high σ of the leakage-free electrolyte is the key factor, leading to the development of the non-volatile electro-magnetic phase switching device of $SrCoO_x$ TFT.

SUPPLEMENTARY MATERIAL

See supplementary material for grazing-incidence X-ray reflectivity analysis of amorphous $NaTaO_3$ films deposited under various oxygen pressures.

ACKNOWLEDGMENTS

We thank N. Hirai for the TEM/STEM analyses. The TEM/STEM analyses, conducted at the Hokkaido Univ., were supported by the Nanotechnology Platform Program from MEXT. T.K. was supported by PRESTO, JST (JPMJPR16R1), Grant-in-Aid for Young Scientists A (15H05543), and Grant-in-Aid for Challenging Exploratory Research (16K14377) from JSPS. H.O. was supported by the Grant-in-Aid for Scientific Research A (25246023) and Grant-in-Aid for Scientific Research on Innovative Areas (25106007) from JSPS.

[1]J. Mannhart and D. G. Schlom, Nature **430**, 620–621 (2004).
[2]E. Dagotto, Science **309**, 257–262 (2005).
[3]H. Takagi and H. Y. Hwang, Science **327**, 1601–1602 (2010).
[4]S. K. Deb, Philos. Mag. **27**, 801–822 (1973).
[5]J. D. Jorgensen, B. W. Veal, A. P. Paulikas, L. J. Nowicki, G. W. Crabtree, H. Claus, and W. K. Kwok, Phys. Rev. B **41**, 1863–1877 (1990).
[6]A. F. Wells, *Structural Inorganic Chemistry*, 5th ed. (Oxford University Press, Oxford, 1984).
[7]C. H. Ahn, A. Bhattacharya, M. Di Ventra, J. N. Eckstein, C. D. Frisbie, M. E. Gershenson, A. M. Goldman, I. H. Inoue, J. Mannhart, A. J. Millis, A. F. Morpurgo, D. Natelson, and J.-M. Triscone, Rev. Mod. Phys. **78**, 1185–1212 (2006).
[8]T. Takeda, Y. Yamaguchi, and H. Watanabe, J. Phys. Soc. Jpn. **33**, 970–972 (1972).
[9]T. Takeda and H. Watanabe, J. Phys. Soc. Jpn. **33**, 973–978 (1972).
[10]S. Balamurugan, K. Yamaura, A. B. Karki, D. P. Young, M. Arai, and E. Takayama-Muromachi, Phys. Rev. B **74**, 172406 (2006).
[11]J. Mizusaki, S. Yamauchi, K. Fueki, and A. Ishikawa, Solid State Ionics **12**, 119–124 (1984).
[12]Z. Shao and S. M. Haile, Nature **431**, 170–173 (2004).
[13]R. Merkle and J. Maier, Angew. Chem. Int. Ed. **47**, 3874–3894 (2008).
[14]H. Jeen, W. S. Choi, M. D. Biegalski, C. M. Folkman, I.-C. Tung, D. D. Fong, J. W. Freeland, D. Shin, H. Ohta, M. F. Chisholm, and H. N. Lee, Nat. Mater. **12**, 1057–1063 (2013).
[15]S. Hu, Y. Wang, C. Cazorla, and J. Seidel, Chem. Mater. **29**, 708–717 (2017).
[16]J.-C. Grenier, A. Wattiaux, J.-P. Doumerc, P. Dordor, L. Fournes, J.-P. Chaminade, and M. Pouchard, J. Solid State Chem. **96**, 20–30 (1992).
[17]P. Bezdicka, A. Wattiaux, J. C. Grenier, M. Pouchard, and P. Hagenmuller, Z. Anorg. Allg. Chem. **619**, 7–12 (1993).
[18]A. Nemudry, P. Rudolf, and R. Schöllhorn, Chem. Mater. **8**, 2232–2238 (1996).
[19]N. Ichikawa, M. Iwanowska, M. Kawai, C. Calers, W. Paulus, and Y. Shimakawa, Dalton Trans. **41**, 10507–10510 (2012).
[20]O. T. Tambunan, M. Y. Lee, D. H. Kim, K. J. Parwanta, and C. U. Jung, J. Korean Phys. Soc. **64**, 1845–1848 (2014).
[21]S. Hu and J. Seidel, Nanotechnology **27**, 325301 (2016).
[22]H. Ohta, Y. Sato, T. Kato, S. W. Kim, K. Nomura, Y. Ikuhara, and H. Hosono, Nat. Commun. **1**, 118 (2010).
[23]T. Katase, K. Endo, T. Tohei, Y. Ikuhara, and H. Ohta, Adv. Electron. Mater. **1**, 1500063 (2015).
[24]T. Katase, Y. Suzuki, and H. Ohta, Adv. Electron. Mater. **2**, 1600044 (2016).
[25]T. Katase, T. Onozato, M. Hirono, T. Mizuno, and H. Ohta, Sci. Rep. **6**, 25819 (2016).
[26]T. Katase, K. Endo, and H. Ohta, APL Mater. **5**, 056105 (2017).
[27]P. G. Dickens and M. S. Whittingham, Q. Rev. Chem. Soc. **22**, 30–44 (1968).
[28]When the porosity of the CAN film reaches ~30% with respect to the fully dense $12CaO{\cdot}7Al_2O_3$ film, the nanopores connect with each other, leading to the percolation conduction of water in the solid CAN film.
[29]T. S. Light, S. Licht, A. C. Bevilacqua, and K. R. Morash, Electrochem. Solid-State Lett. **8**, E16–E19 (2005).
[30]T. Katase, K. Endo, and H. Ohta, Phys. Rev. B **90**, 161105(R) (2014).
[31]T. Katase, K. Endo, and H. Ohta, Phys. Rev. B **92**, 035302 (2015).
[32]H. Ohta, J. Mater. Sci. **48**, 2797–2805 (2013).